# Combined Compact Difference Scheme for Linear Second-Order Partial Differential Equations with Mixed Derivative ☆

Spike T. Lee[a], Jun Liu[b], Hai-Wei Sun[c,*]

[a] *Department of Mathematics, The Chinese University of Hong Kong, Shatin, Hong Kong, China*
[b] *Department of Mathematics, Southern Illinois University, Carbondale, IL, USA*
[c] *Department of Mathematics, University of Macau, Macao, China*

**Abstract**

A combined compact difference scheme is proposed for linear second-order partial differential equations with mixed derivative. The scheme is based on a nine-point stencil at interior with sixth-order accurate local truncation error. Fourier analysis is used to analyze the spectral resolution of the proposed scheme. Numerical tests demonstrate at least sixth-order convergence rate with Dirichlet boundary condition and fifth-order with Robin boundary condition. A bonus is that high Reynolds numbers do not interfere with the order of accuracy.

*Keywords:* combined compact difference scheme, two dimensional, partial differential equations, mixed derivative, high-order finite difference, Fourier error analysis
*2000 MSC:* 65N06, 65F50

## 1. Introduction

In this paper we aim to find a high-order compact (HOC) scheme for the general two dimensional (2D) linear partial differential equation (PDE)

☆The research was partially supported by the research grants 033/2009/A and 005/2012/A1 from FDCT of Macao, MYRG206(Y1-L4)-FST11-SHW from University of Macau.

*Corresponding author
*Email addresses:* spiketlee@gmail.com (Spike T. Lee), gdctor@gmail.com (Jun Liu), HSun@umac.mo (Hai-Wei Sun)

with a mixed derivative

$$\nabla \cdot (\mathsf{K}\nabla u) + \mathsf{D} \cdot \nabla u + \alpha u = g(x, y), \quad (x, y) \in \Omega. \tag{1.1}$$

The domain $\Omega$ is rectangular and there is a suitable boundary condition defined on its boundary $\partial\Omega$. The functions $u$ and $g$ are assumed to be sufficiently smooth and have continuous partial derivatives up to necessary orders. In particular, $\mathsf{D}$ in (1.1) denotes the horizontal velocity field, and $\mathsf{K}$ is represented in a Cartesian coordinate system as a tensor. The tensor $\mathsf{K}$ is assumed to possess nonzero off-diagonal elements such that (1.1) yields a mixed derivative. In reality, such characteristics exists in modeling porous media flow in reservoir simulation [2, 11, 24], where $\mathsf{K}$ is also known as a conductivity tensor representing the permeability field, and it is very likely that $\mathsf{K}$ contains nonzero off-diagonal components.

Equation (1.1) originates from other aspects as well. For instance, the mixed derivative appears when one transforms a knotty non-rectangular domain into a convenient rectangular one [1, 8, 29]. Besides, transforming a nonuniform grid into a uniform one also contributes the mixed derivative to the governing equation [12]. On the other hand, there are many real-life applications which involve the 2D parabolic equations with a mixed derivative. Perfectly matched layers (PML) are studied for a 2D coupled nonlinear Schrödinger system with mixed derivatives in the modeling of gap solitons, where the constructed PML can be used to soothe the waves which travel through the boundary [7]. Before laying hands on the parabolic equation, it is often the practice to start by studying its steady-state case, namely the PDE (1.1). Also it is shown in [7] that the removal of the mixed derivative is not always attainable. Therefore, it is inevitable to face (1.1) directly. However, the presence of the mixed derivative makes (1.1) thorny to handle. For example, conventional central difference scheme is easy to implement but only has second-order convergence.

Above all, one might pursue a high-order accurate numerical solution for (1.1), especially in large scale modelings. The purpose of using high-order schemes lies in using a much coarser grid (a smaller system size) to obtain high-order approximations. Several high-order schemes were once proposed to solve equations like (1.1). For instance, standard high-order finite difference schemes are usable but they have a wider stencil and lead to coefficient matrices with larger bandwidth. In [19, 25], a family of high-order methods is used to solve (1.1). The idea is to exploit many values of the known function $g(x, y)$ (the right-hand side of (1.1)) at grid points as well as non-grid points. However, these methods are not easily generalizable

to the parabolic equations. On the other hand, HOC schemes are popular among practitioners because they only utilize a 9-point stencil at any 2D reference grid point. As a result, there exists a favorable sparsity pattern in resulting coefficient matrices. Also the compact structure is adaptable to local mesh refinement strategy, and good at handling boundary grid points. Nevertheless, equations with mixed derivative like (1.1) are hot potatoes for HOC schemes as well [12]. Recently, Fournié and Karaa [10] broke the curse and derived a 9-point fourth-order compact (FOC) finite difference scheme for a 2D PDE with mixed derivative and constant coefficients. Later on, this result is extended to the case with variable coefficients [15] and to the three dimensional case [16]. However, the 2D FOC scheme in [10, 15] requires second derivatives to have the same coefficient, i.e., the main diagonal of $\mathsf{K}$ in (1.1) is identical. Furthermore, fourth-order convergence is obtained in [10, 15, 16] when the Reynolds number is not too high.

Most of the HOC schemes are called *explicit* since they approximate the derivatives by the nodal values of the target function. To solve (1.1), we are interested in another branch of HOC schemes, which are known as the *implicit* HOC schemes. The core of such schemes is to treat the derivatives as unknowns simultaneously along with the solution. The implicit HOC schemes are known to have better spectral resolution, and they can attain high-order accuracy by using additional information of the derivatives. Furthermore, implicit HOC schemes are highly flexible to use because they are mainly composed of fixed difference equations which connect the nodal values of the original function and its derivatives. These difference equations are independent from the governing equation, and no specific care needs to be taken when the subject of interest changes. Also the implicit treatment of derivatives allows us to handle the Robin boundary condition more conveniently. One prominent example of implicit HOC schemes is the combined compact difference (CCD) scheme proposed by Chu and Fan [5], which can be regarded as an extension of the standard Padé schemes discussed by Lele [17]. A similar idea is also mentioned by Mahesh [20], where the implicit treatment is referred to as the coupled-derivative (C-D) schemes. In [5], the CCD scheme is derived by using local Hermitian polynomials and is a one dimensional (1D) 3-point sixth-order finite difference scheme. Fourier analysis shows that the CCD scheme has better spectral resolution than many other existing compact or noncompact high-order schemes. Nevertheless, only an alternating direction implicit (ADI) scheme is used in [5] to reduce the 2D case to 1D such that the CCD scheme is feasible. In other words, the 2D case is not directly tackled in [5], not to mention the intrusion of mixed derivative. Later on, Sengupta et al. [26, 27] extend the CCD scheme to

2D for computing wave propagation problems and Navier-Stokes equation. However, the mixed derivative term is not yet involved in there.

In this paper, we extend the work in [5] and propose a 2D combined compact difference (CCD2) scheme to solve linear second-order partial differential equations with mixed derivative. The scheme is based on a 9-point stencil at interior and has sixth-order accurate local truncation order. For non-periodic boundary condition, additional difference equations are needed at the boundary grid points. We suggest a group of finite difference equations at the boundary which have slightly lower truncation errors than the interior. Following [5, 17], we use the Fourier analysis to check the spectral resolution of the proposed scheme. In numerical experiments, we compare the CCD2 scheme with existing schemes for solving 2D PDEs with a mixed derivative, for instance, the standard central difference scheme and the fourth-order accurate FOC scheme in [15]. Numerical tests demonstrate that the CCD2 scheme achieves at least sixth-order convergence rate when solving (1.1) with Dirichlet boundary condition, and fifth-order with Robin boundary condition. In addition, we observe from numerical experiments that high Reynolds numbers do not hinder the CCD2 scheme, which is an unexpected advantage over the FOC method in [15]. Our paper is arranged as follows. In Section 2, we introduce the CCD2 framework and consider different treatment for interior and boundary grid points. We also discuss the special structure of the coefficient matrix when the governing equation has a periodic boundary condition. In Section 3, we carry out the Fourier analysis of errors to characterize the spectral resolution. In Section 4, we pull out the numerical experiments, test the CCD2 scheme in examples coming from different literatures, and compare the CCD2 scheme with other existing discretization methods for (1.1). In Section 5, we bring down the curtain on the paper and give some promising ideas about follow-ups.

## 2. CCD2 scheme formulation

To establish the CCD2 scheme, we rewrite (1.1) into a more natural form

$$d_1 u + d_2 \frac{\partial u}{\partial x} + d_3 \frac{\partial^2 u}{\partial x^2} + d_4 \frac{\partial u}{\partial y} + d_5 \frac{\partial^2 u}{\partial y^2} + d_6 \frac{\partial^2 u}{\partial x \partial y} = g(x, y), \quad (x, y) \in \Omega, \tag{2.1}$$

where $d_1$, $d_2$, $d_3$, $d_4$, $d_5$, and $d_6$ are functions of $x$ and $y$ having continuous partial derivatives up to necessary orders. In this paper, we consider a function $u(x, y)$ defined on a rectangular domain $\Omega = [0, l_x] \times [0, l_y]$. For

convenience, we symbolize the derivatives by $\{u, u^x, u^{xx}, u^y, u^{yy}, u^{xy}\}$ respectively. For (2.1), we consider the general Robin boundary condition

$$a_1 u + a_2 \frac{\partial u}{\partial \mathbf{n}} = g_0(x, y), \quad (x, y) \in \partial\Omega, \tag{2.2}$$

where $\partial\Omega$ is the boundary of $\Omega$, $a_1$, $a_2$, and $g_0$ are functions of $x$ and $y$ defined on $\partial\Omega$, and $\partial u/\partial \mathbf{n}$ denotes the normal derivative at $\partial\Omega$. We discretize $\Omega$ by a uniform Cartesian grid

$$\Phi = \Big\{(x_j, y_k) = ((j-1)h_x, (k-1)h_y) : j = 1, 2, \ldots, N_x, k = 1, 2, \ldots, N_y\Big\},$$

where $N_x$ and $N_y$ are the numbers of grid points in the $x$- and $y$-directions, and

$$h_x = \frac{l_x}{N_x - 1} \quad \text{and} \quad h_y = \frac{l_y}{N_y - 1}$$

are the corresponding step sizes. Note that boundary grid points ($j = 1, N_x$ or $k = 1, N_y$) are included in the computational domain $\Phi$. One advantage of including boundary grid points as unknowns lies in its flexible treatment of the general boundary condition [18].

The CCD2 scheme also belongs to the family of implicit HOC schemes. For implicit schemes, the derivatives are reckoned as variables along with the target function $u$. Owing to the mixed derivative term in (2.1), we have to treat $u$ and its five derivatives as variables. Let

$$\{u_{j,k}, u^x_{j,k}, u^{xx}_{j,k}, u^y_{j,k}, u^{yy}_{j,k}, u^{xy}_{j,k}\}$$

denote the approximate values of functions $\{u, u^x, u^{xx}, u^y, u^{yy}, u^{xy}\}$ at $(x_j, y_k) \in \Phi$ respectively.

In the following, we will discuss how to implement the CCD2 scheme on $\Phi$. Note that grid points at different locations require different treatment. Therefore we first divide the grid points in $\Phi$ into two groups: the interior grid points and the boundary grid points; see Figure 1.

### *2.1. CCD2 scheme for interior grid points*

For each interior grid point $(x_j, y_k)$ ($j = 2, \ldots, N_x - 1, k = 2, \ldots, N_y - 1$), there are 6 unknowns $\{u_{j,k}, u^x_{j,k}, u^{xx}_{j,k}, u^y_{j,k}, u^{yy}_{j,k}, u^{xy}_{j,k}\}$ to be determined and consequently we should provide 6 independent difference equations. Meanwhile, only nodal values of $\{u, u^x, u^y, u^{xy}, u^{xx}, u^{yy}\}$ are allowed to appear in such difference equations. To keep the structure compact, we only consider nodal values at an interior grid point $(x_j, y_k)$ and its 8 neighboring grid points, which is also known as a 9-point stencil in 2D case.

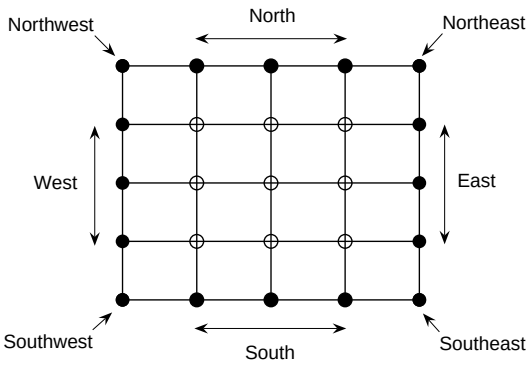


Figure 1: Interior grid points (○) and boundary grid points (●).

The governing equation (2.1) at $(x_j, y_k)$

$$\begin{aligned} & d_1(x_j,y_k)u_{j,k} + d_2(x_j,y_k)u^x_{j,k} + d_3(x_j,y_k)u^{xx}_{j,k} \\ & +d_4(x_j,y_k)u^y_{j,k} + d_5(x_j,y_k)u^{yy}_{j,k} + d_6(x_j,y_k)u^{xy}_{j,k} \quad = \quad g(x_j,y_k) \end{aligned} \tag{2.3}$$

is a prior choice since it provides the exact relation. Note that the original 3-point sixth-order CCD scheme proposed in [5] comprises two groups of 1D difference equations for interior grid points. Since these equations achieve sixth-order accuracy in [5] and can easily be generalized to the 2D case, we simply borrow them and put on some 2D notations. For an interior grid point, these difference equations become

$$\begin{aligned} & \frac{15}{h_x^2}(u_{j-1,k} - u_{j+1,k}) + \frac{1}{h_x}(7u^x_{j-1,k} + 16u^x_{j,k} + 7u^x_{j+1,k}) + u^{xx}_{j-1,k} - u^{xx}_{j+1,k} \\ =& \mathcal{O}(h_x^5), \end{aligned} \tag{2.4a}$$

$$\begin{aligned} & \frac{24}{h_x^2}(u_{j-1,k} - 2u_{j,k} + u_{j+1,k}) + \frac{9}{h_x}(u^x_{j-1,k} - u^x_{j+1,k}) + u^{xx}_{j-1,k} - 8u^{xx}_{j,k} + u^{xx}_{j+1,k} \\ =& \mathcal{O}(h_x^6) \end{aligned} \tag{2.4b}$$

along the $x$-direction and

$$\begin{aligned} & \frac{15}{h_y^2}(u_{j,k-1} - u_{j,k+1}) + \frac{1}{h_y}(7u^y_{j,k-1} + 16u^y_{j,k} + 7u^y_{j,k+1}) + u^{yy}_{j,k-1} - u^{yy}_{j,k+1} \\ =& \mathcal{O}(h_y^5), \end{aligned} \tag{2.5a}$$

$$\begin{aligned} & \frac{24}{h_y^2}(u_{j,k-1} - 2u_{j,k} + u_{j,k+1}) + \frac{9}{h_y}(u^y_{j,k-1} - u^y_{j,k+1}) + u^{yy}_{j,k-1} - 8u^{yy}_{j,k} + u^{yy}_{j,k+1} \\ =& \mathcal{O}(h_y^6) \end{aligned} \tag{2.5b}$$

along the $y$-direction. The equations (2.4) and (2.5) link the nodal values of $u$, its first and second derivatives by a 3-point stencil, which is a special case of 9-point stencil and does not violate the compact structure.

The above equations (2.4) and (2.5) together with (2.3) already yield five independent equations for an interior grid point $(x_j, y_k)$. Thus, we still lack one equation regarding the remaining member, the mixed derivative term $u^{xy}_{j,k}$. We suggest the following three different approximations ranging from second-order accuracy to sixth-order.

A natural thought is to use the standard second-order central difference approximation

$$u^{xy}_{j,k} = \frac{1}{4h_x h_y}(u_{j+1,k+1} - u_{j-1,k+1} + u_{j-1,k-1} - u_{j+1,k-1}) + \mathcal{O}(h_x^2 + h_y^2), \quad (2.6)$$

where no information of the derivatives at neighboring nodes is used. This second-order approximation will result in a second-order accurate CCD2 scheme. Higher-order approximations must be used in order to achieve better accuracy.

By the 2D Taylor expansions of $u$, we derive a fourth-order accurate approximation to the mixed derivative

$$\begin{aligned} u^{xy}_{j,k} &= -\frac{1}{4h_x h_y}(u_{j+1,k+1} - u_{j-1,k+1} + u_{j-1,k-1} - u_{j+1,k-1}) \\ &\quad + \frac{1}{2h_y}(u^x_{j,k+1} - u^x_{j,k-1}) + \frac{1}{2h_x}(u^y_{j+1,k} - u^y_{j-1,k}) \\ &\quad + \mathcal{O}(h_x^4 + h_y^4), \end{aligned} \quad (2.7)$$

which will lead to a fourth-order accurate CCD2 scheme. We remark that this approximation uses the additional nodal values of the first derivatives $u^x$ and $u^y$.

The motivation of passing fourth-order accuracy is that the original CCD scheme [5] attains sixth-order accuracy. In a similar way, we propose a sixth-order accurate approximation to the mixed derivative

$$\begin{aligned} u^{xy}_{j,k} &= -\frac{9}{32h_x h_y}(u_{j+1,k+1} - u_{j-1,k+1} + u_{j-1,k-1} - u_{j+1,k-1}) \\ &\quad + \frac{9}{16h_y}(u^x_{j,k+1} - u^x_{j,k-1}) + \frac{9}{16h_x}(u^y_{j+1,k} - u^y_{j-1,k}) \\ &\quad - \frac{1}{32}\Big(2u^{xy}_{j+1,k} + 2u^{xy}_{j,k+1} + 2u^{xy}_{j-1,k} + 2u^{xy}_{j,k-1} \\ &\quad - u^{xy}_{j+1,k+1} - u^{xy}_{j-1,k+1} - u^{xy}_{j-1,k-1} - u^{xy}_{j+1,k-1}\Big) \\ &\quad + \mathcal{O}(h_x^6 + h_y^6), \end{aligned} \quad (2.8)$$

with which we can finally derive a sixth-order accurate CCD2 scheme. Also, this approximation extra employs the information of the mixed derivative $u^{xy}$.

The first second-order approximation (2.6) is well-known already [14], while the latter two are seldom considered in standard finite difference schemes. Note that (2.6), (2.7), and (2.8) are of 9-point stencil, which keeps the compact feature of interior difference equations. The derivation of (2.6), (2.7), and (2.8) will be given in Appendix A.

To illustrate our difference equations with mixed derivative more succinctly, we introduce the following general 9-point $r$th-order accurate compact difference equation

$$\sum_{p=j-1}^{j+1}\sum_{q=k-1}^{k+1}\left(\frac{s_{p,q}u_{p,q}}{h_xh_y}+\frac{s^x_{p,q}u^x_{p,q}}{h_y}+\frac{s^y_{p,q}u^y_{p,q}}{h_x}+s^{xy}_{p,q}u^{xy}_{p,q}\right)=\mathcal{O}(h_x^r+h_y^r). \quad (2.9)$$

The equation (2.9) is determined by the four coefficient stencils as follows:

$$S=\begin{bmatrix} s_{j-1,k+1} & s_{j,k+1} & s_{j+1,k+1}\\ s_{j-1,k} & s_{j,k} & s_{j+1,k}\\ s_{j-1,k-1} & s_{j,k-1} & s_{j+1,k-1}\end{bmatrix},\quad S^x=\begin{bmatrix} s^x_{j-1,k+1} & s^x_{j,k+1} & s^x_{j+1,k+1}\\ s^x_{j-1,k} & s^x_{j,k} & s^x_{j+1,k}\\ s^x_{j-1,k-1} & s^x_{j,k-1} & s^x_{j+1,k-1}\end{bmatrix},$$

$$S^y=\begin{bmatrix} s^y_{j-1,k+1} & s^y_{j,k+1} & s^y_{j+1,k+1}\\ s^y_{j-1,k} & s^y_{j,k} & s^y_{j+1,k}\\ s^y_{j-1,k-1} & s^y_{j,k-1} & s^y_{j+1,k-1}\end{bmatrix},\quad S^{xy}=\begin{bmatrix} s^{xy}_{j-1,k+1} & s^{xy}_{j,k+1} & s^{xy}_{j+1,k+1}\\ s^{xy}_{j-1,k} & s^{xy}_{j,k} & s^{xy}_{j+1,k}\\ s^{xy}_{j-1,k-1} & s^{xy}_{j,k-1} & s^{xy}_{j+1,k-1}\end{bmatrix}.$$

For instance, (2.8) is written in the following form according to (2.9)

$$S=\begin{bmatrix}9&0&-9\\0&0&0\\-9&0&9\end{bmatrix}, S^x=\begin{bmatrix}0&18&0\\0&0&0\\0&-18&0\end{bmatrix}, S^y\begin{bmatrix}0&0&0\\-18&0&18\\0&0&0\end{bmatrix}, S^{xy}=\begin{bmatrix}1&-2&1\\-2&-32&-2\\1&-2&1\end{bmatrix}.$$

Note that all the above entries in $S$, $S^x$, $S^y$, and $S^{xy}$ have been scaled for a neat formulation.

Now every single interior grid point is related to 6 difference equations, namely (2.3), (2.4), (2.5), and (2.8). In particular, we would like to demonstrate the case when the governing equation (2.1) has a periodic boundary condition. In such case, the coefficient matrix of CCD2 scheme can be explicitly presented. Due to periodicity, we need to determine the unknowns $\{u_{j,k}, u^x_{j,k}, u^{xx}_{j,k}, u^y_{j,k}, u^{yy}_{j,k}, u^{xy}_{j,k}\}$ only on

$$\mathring{\Phi}=\Phi\backslash\Big\{(x_j,y_k)=((j-1)h_x,(k-1)h_y): j=N_x \text{ or } k=N_y\Big\},$$

which is the original computational grid $\Phi$ minus the grid points at East, North, Northeast, Northwest, and Southeast boundaries. Note that the number of computational grid points in $\mathring{\Phi}$ is $(N_x-1)(N_y-1)$. For clarity of notations, we assume $n_x = N_x - 1$ and $n_y = N_y - 1$ for the moment. For periodic boundary condition, every grid point in the computational grid $\mathring{\Phi}$ can be regarded as an interior grid point. It is because each $(x_k, y_k) \in \mathring{\Phi}$ can form a 9-point stencil within $\mathring{\Phi}$. Therefore we only have to use the interior difference equations.

To write the CCD2 system in a concise style, we proceed to define several notations. Let the vectorization of a matrix $A = [a_{j,k}]_{m\times n} \in \mathbb{R}^{m\times n}$ be defined as

$$\mathrm{vec}(A) = (a_{11}, \ldots, a_{m1}, a_{12}, \ldots, a_{m2}, \ldots, a_{1n}, \ldots, a_{mn})^{\mathsf{T}}.$$

An $n$-by-$n$ circulant matrix determined by 3 elements is defined by

$$\mathcal{C}(a,b,c)_n \equiv \begin{bmatrix} b & c & \cdots & 0 & a \\ a & b & c & \cdots & 0 \\ \vdots & \ddots & \ddots & \ddots & \vdots \\ 0 & \cdots & a & b & c \\ c & \cdots & 0 & a & b \end{bmatrix} \in \mathbb{R}^{n\times n}.$$

Let $I_n$ be an $n$-by-$n$ identity matrix, and $I_n^+, I_n^-$ be two special circulant matrices

$$I_n^+ = \mathcal{C}(1,0,1)_n \quad \text{and} \quad I_n^- = \mathcal{C}(-1,0,1)_n.$$

Unlike the way of gathering all unknowns at a grid point into one sub-block [5], which is more suitable for the 1D case, we order all the unknowns in the natural column-wise sense

$$\boldsymbol{u} = \mathrm{vec}\left(\begin{bmatrix} \boldsymbol{v} & \boldsymbol{v}^x & \boldsymbol{v}^{xx} & \boldsymbol{v}^y & \boldsymbol{v}^{yy} & \boldsymbol{v}^{xy} \end{bmatrix}\right),$$

where

$$\begin{aligned} \boldsymbol{v} &= \mathrm{vec}([u_{j,k}]_{n_x\times n_y}), \quad & \boldsymbol{v}^x &= \mathrm{vec}([u^x_{j,k}]_{n_x\times n_y}), \quad & \boldsymbol{v}^{xx} &= \mathrm{vec}([u^{xx}_{j,k}]_{n_x\times n_y}), \\ \boldsymbol{v}^y &= \mathrm{vec}([u^y_{j,k}]_{n_x\times n_y}), \quad & \boldsymbol{v}^{yy} &= \mathrm{vec}([u^{yy}_{j,k}]_{n_x\times n_y}), \quad & \boldsymbol{v}^{xy} &= \mathrm{vec}([u^{xy}_{j,k}]_{n_x\times n_y}). \end{aligned}$$

Similarly, let $\boldsymbol{g} = \mathrm{vec}([g(x_j, y_k)]_{n_x\times n_y})$ contain the values of right-hand side forcing term on $\mathring{\Phi}$. Also let $\otimes$ be the Kronecker product [13]. Using the above notations and collecting the 6 interior difference equations (2.3), (2.4), (2.5),

and (2.8), we finally obtain the whole CCD2 linear system

$$A\boldsymbol{u} \equiv \begin{bmatrix} B_{1,1} & B_{1,2} & B_{1,3} & B_{1,4} & B_{1,5} & B_{1,6} \\ B_{2,1} & B_{2,2} & B_{2,3} & 0 & 0 & 0 \\ B_{3,1} & B_{3,2} & B_{3,3} & 0 & 0 & 0 \\ B_{4,1} & 0 & 0 & B_{4,4} & B_{4,5} & 0 \\ B_{5,1} & 0 & 0 & B_{5,4} & B_{5,5} & 0 \\ B_{6,1} & B_{6,2} & 0 & B_{6,4} & 0 & B_{6,6} \end{bmatrix} \begin{bmatrix} \boldsymbol{v} \\ \boldsymbol{v}^x \\ \boldsymbol{v}^{xx} \\ \boldsymbol{v}^y \\ \boldsymbol{v}^{yy} \\ \boldsymbol{v}^{xy} \end{bmatrix} = \begin{bmatrix} \boldsymbol{g} \\ \boldsymbol{0} \\ \boldsymbol{0} \\ \boldsymbol{0} \\ \boldsymbol{0} \\ \boldsymbol{0} \end{bmatrix} \equiv \boldsymbol{b}. \quad (2.10)$$

The blocks are $B_{1,q} = \operatorname{diag}\left(\operatorname{vec}([d_q(x_j, y_k)]_{n_x \times n_y})\right),\ q = 1, \ldots, 6,$

$$\begin{array}{lll} B_{2,1} = -15I^-_{n_x} \otimes I_{n_y}, & B_{2,2} = C^1_{n_x} \otimes I_{n_y}, & B_{2,3} = -I^-_{n_x} \otimes I_{n_y}, \\ B_{3,1} = 24C^2_{n_x} \otimes I_{n_y}, & B_{3,2} = -9I^-_{n_x} \otimes I_{n_y}, & B_{3,3} = C^3_{n_x} \otimes I_{n_y}, \\ B_{4,1} = I_{n_x} \otimes -15I^-_{n_y}, & B_{4,4} = I_{n_x} \otimes C^1_{n_y}, & B_{4,5} = I_{n_x} \otimes -I^-_{n_y}, \\ B_{5,1} = I_{n_x} \otimes 24C^2_{n_y}, & B_{5,4} = I_{n_x} \otimes -9I^-_{n_y}, & B_{5,5} = I_{n_x} \otimes C^3_{n_y}, \\ B_{6,1} = I^-_{n_x} \otimes 9I^-_{n_y}, & B_{6,2} = I_{n_x} \otimes 18I^-_{n_y} & B_{6,4} = I^-_{n_x} \otimes C^4_{n_y}, \end{array}$$

$$B_{6,6} = I^+_{n_x} \otimes C^2_{n_y} + I_{n_x} \otimes \mathcal{C}(-2, -32, -2)_{n_y},$$

where

$$C^1_n = \mathcal{C}(7, 16, 7)_n, \quad C^2_n = \mathcal{C}(1, -2, 1)_n,$$
$$C^3_n = \mathcal{C}(1, -8, 1)_n, \quad \text{and} \quad C^4_n = \mathcal{C}(0, -18, 0)_n.$$

*2.2. CCD2 scheme for boundary grid points*

In the last subsection, 6 difference equations have been developed for each interior grid point. Particularly, the resulting CCD2 system is written in an explicit form (2.10) when (2.1) has a periodic boundary condition. For a general boundary condition like (2.2), the proposed CCD2 scheme includes boundary grid points as unknowns, which handles (2.2) easily but complicates the system construction inevitably. It is because the interior difference equations are not applicable to boundary grid points. To close the system, or find the corresponding 6 equations for each boundary grid point, we have to design an extra set of boundary difference equations.

The first natural choice is to use the governing equation (2.3) at the boundary grid points. For instance, the 1D CCD scheme in [5] employs this idea, where the governing equation, its boundary condition, and an additional boundary difference equation are used at the boundary. However, in some cases, (2.3) will be nullified when the coefficient functions $d_q,\ q = 1, \ldots, 6$, vanish at the boundary. To make the CCD2 scheme more inclusive,

we only utilize the general boundary condition (2.2) at $(x_j, y_k)$ ($j = 1, N_x$ or $k = 1, N_y$)

$$a_1(x_j, y_k)u_{j,k} + a_2(x_j, y_k)\left[\frac{\partial u}{\partial \mathbf{n}}\right]_{j,k} = g_0(x_j, y_k). \tag{2.11}$$

From (2.11), we see that the Robin boundary condition is easily handled without any discretization owing to the implicit characteristics of the CCD2 scheme.

We remark here that the boundary grid points at East, North, West, and South are boundary grid points in one direction but interior in another direction; see Figure 1. For instance, a grid point belonging to the East boundary is at the end of $x$-direction, but not $y$-direction. Therefore the two interior difference equations in (2.5) along the $y$-direction still work for grid points at the East boundary. In this regard, we need 3 more difference equations for East, North, West, and South, and 5 more for Northeast, Northwest, Southwest, and Southeast. According to previous literatures [5, 20], boundary closures are not required to be as high-order as the interior. Therefore we first propose the following fourth-order accurate difference equations:

East/Northeast/Southeast: $j = N_x, k = 1, \ldots, N_y$

$$\begin{aligned}&\frac{1}{h_x^2}(u_{j-2,k} - 32u_{j-1,k} + 31u_{j,k}) - \frac{1}{h_x}(16u^x_{j-1,k} + 14u^x_{j,k}) - 2(2u^{xx}_{j-1,k} - u^{xx}_{j,k})\\ =&\mathcal{O}(h_x^4),\end{aligned} \tag{2.12a}$$

$$\begin{aligned}&\frac{1}{h_x^2}(u_{j-3,k} + 18u_{j-2,k} - 9u_{j-1,k} - 10u_{j,k}) + \frac{3}{h_x}(3u^x_{j-2,k} + 6u^x_{j-1,k} + u^x_{j,k})\\ =&\mathcal{O}(h_x^4).\end{aligned} \tag{2.12b}$$

North/Northeast/Northwest: $j = 1, \ldots, N_x, k = N_y$

$$\begin{aligned}&\frac{1}{h_y^2}(u_{j,k-2} - 32u_{j,k-1} + 31u_{j,k}) - \frac{1}{h_y}(16u^y_{j,k-1} + 14u^y_{j,k}) - 2(2u^{yy}_{j,k-1} - u^{yy}_{j,k})\\ =&\mathcal{O}(h_y^4),\end{aligned} \tag{2.13a}$$

$$\begin{aligned}&\frac{1}{h_y^2}(u_{j,k-3} + 18u_{j,k-2} - 9u_{j,k-1} - 10u_{j,k}) + \frac{3}{h_y}(3u^y_{j,k-2} + 6u^y_{j,k-1} + u^y_{j,k})\\ =&\mathcal{O}(h_y^4).\end{aligned} \tag{2.13b}$$

West/Northwest/Southwest: $j = 1, k = 1, \ldots, N_y$

$$\frac{1}{h_x^2}(31u_{j,k} - 32u_{j+1,k} + u_{j+2,k}) + \frac{1}{h_x}(14u^x_{j,k} + 16u^x_{j+1,k}) + 2(u^{xx}_{j,k} - 2u^{xx}_{j+1,k}) = \mathcal{O}(h_x^4), \tag{2.14a}$$

$$\frac{1}{h_x^2}(10u_{j,k} + 9u_{j+1,k} - 18u_{j+2,k} - u_{j+3,k}) + \frac{3}{h_x}(u^x_{j,k} + 6u^x_{j+1,k} + 3u^x_{j+2,k}) = \mathcal{O}(h_x^4). \tag{2.14b}$$

South/Southwest/Southeast: $j = 1, \ldots, N_x, k = 1$

$$\frac{1}{h_y^2}(31u_{j,k} - 32u_{j,k+1} + u_{j,k+2}) + \frac{1}{h_y}(14u^y_{j,k} + 16u^y_{j,k+1}) + 2(u^{yy}_{j,k} - 2u^{yy}_{j,k+1}) = \mathcal{O}(h_y^4), \tag{2.15a}$$

$$\frac{1}{h_y^2}(10u_{j,k} + 9u_{j,k+1} - 18u_{j,k+2} - u_{j,k+3}) + \frac{3}{h_y}(u^y_{j,k} + 6u^y_{j,k+1} + 3u^y_{j,k+2}) = \mathcal{O}(h_y^4). \tag{2.15b}$$

With 3 or 4 grid points along one direction, the above boundary difference equations are not strictly compact in the traditional sense, but they are necessary to retain the high-order accuracy of the entire CCD2 scheme. Nevertheless, we remark that these equations are only used at boundary grid points. The interior difference equations contributes to the major compact structure.

Till now, one could notice that there are 4 difference equations and a boundary condition (2.11) for each boundary grid point. To close the system, we try to find a remainder regarding the mixed derivative, as we have done for the interior grid points. By the 2D Taylor expansions and some tedious calculations, we are able to deduce some compact difference equations for approximating $u^{xy}_{j,k}$ at the boundary grid points. Using the concise notation in (2.9), we give the corresponding coefficient stencils of a group of fourth-order accurate equations at the four corners:

Northeast: $j = N_x - 1, k = N_y - 1$ in (2.9)

$$S = \begin{bmatrix} 0 & -4 & 4 \\ 0 & 4 & -4 \\ 0 & 0 & 0 \end{bmatrix}, S^x = \begin{bmatrix} 0 & -2 & -2 \\ 0 & 2 & 2 \\ 0 & 0 & 0 \end{bmatrix}, S^y = \begin{bmatrix} 0 & 2 & -2 \\ 0 & 2 & -2 \\ 0 & 0 & 0 \end{bmatrix}, S^{xy} = \begin{bmatrix} 0 & 1 & 1 \\ 0 & 1 & 1 \\ 0 & 0 & 0 \end{bmatrix}. \tag{2.16a}$$

Northwest: $j = 2, k = N_y - 1$ in (2.9)

$$S = \begin{bmatrix} -4 & 4 & 0 \\ 4 & -4 & 0 \\ 0 & 0 & 0 \end{bmatrix}, S^x = \begin{bmatrix} -2 & -2 & 0 \\ 2 & 2 & 0 \\ 0 & 0 & 0 \end{bmatrix}, S^y = \begin{bmatrix} 2 & -2 & 0 \\ 2 & -2 & 0 \\ 0 & 0 & 0 \end{bmatrix}, S^{xy} = \begin{bmatrix} 1 & 1 & 0 \\ 1 & 1 & 0 \\ 0 & 0 & 0 \end{bmatrix}. \tag{2.16b}$$

Southwest: $j = 2, k = 2$ in (2.9)

$$S = \begin{bmatrix} 0 & 0 & 0 \\ -4 & 4 & 0 \\ 4 & -4 & 0 \end{bmatrix}, S^x = \begin{bmatrix} 0 & 0 & 0 \\ -2 & -2 & 0 \\ 2 & 2 & 0 \end{bmatrix}, S^y = \begin{bmatrix} 0 & 0 & 0 \\ 2 & -2 & 0 \\ 2 & -2 & 0 \end{bmatrix}, S^{xy} = \begin{bmatrix} 0 & 0 & 0 \\ 1 & 1 & 0 \\ 1 & 1 & 0 \end{bmatrix}. \tag{2.16c}$$

Southeast: $j = N_x - 1, k = 2$ in (2.9)

$$S = \begin{bmatrix} 0 & 0 & 0 \\ 0 & -4 & 4 \\ 0 & 4 & -4 \end{bmatrix}, S^x = \begin{bmatrix} 0 & 0 & 0 \\ 0 & -2 & -2 \\ 0 & 2 & 2 \end{bmatrix}, S^y = \begin{bmatrix} 0 & 0 & 0 \\ 0 & 2 & -2 \\ 0 & 2 & -2 \end{bmatrix}, S^{xy} = \begin{bmatrix} 0 & 0 & 0 \\ 0 & 1 & 1 \\ 0 & 1 & 1 \end{bmatrix}. \tag{2.16d}$$

The nonzero elements in those coefficient stencils clearly show the compactness of the difference equations, where only the grid points directly adjacent to the corner are selected. For boundary grid points at East, North, West, and South, another group of fourth-order accurate difference equations is built as follows:

East: $j = N_x - 1, k = 2, \ldots, N_y - 1$ in (2.9)

$$S = \begin{bmatrix} 0 & 0 & 0 \\ 0 & 0 & 0 \\ 0 & 0 & 0 \end{bmatrix}, S^x = \begin{bmatrix} 0 & -3 & -3 \\ 0 & 0 & 0 \\ 0 & 3 & 3 \end{bmatrix}, S^y = \begin{bmatrix} 0 & 0 & 0 \\ 0 & 0 & 0 \\ 0 & 0 & 0 \end{bmatrix}, S^{xy} = \begin{bmatrix} 0 & 1 & 1 \\ 0 & 4 & 4 \\ 0 & 1 & 1 \end{bmatrix}. \tag{2.17a}$$

North: $j = 2, \ldots, N_x - 1, k = N_y - 1$ in (2.9)

$$S = \begin{bmatrix} 0 & 0 & 0 \\ 0 & 0 & 0 \\ 0 & 0 & 0 \end{bmatrix}, S^x = \begin{bmatrix} 0 & 0 & 0 \\ 0 & 0 & 0 \\ 0 & 0 & 0 \end{bmatrix}, S^y = \begin{bmatrix} 3 & 0 & -3 \\ 3 & 0 & -3 \\ 0 & 0 & 0 \end{bmatrix}, S^{xy} = \begin{bmatrix} 1 & 4 & 1 \\ 1 & 4 & 1 \\ 0 & 0 & 0 \end{bmatrix}. \tag{2.17b}$$

West: $j = 2, k = 2, \ldots, N_y - 1$ in (2.9)

$$S = \begin{bmatrix} 0 & 0 & 0 \\ 0 & 0 & 0 \\ 0 & 0 & 0 \end{bmatrix}, S^x = \begin{bmatrix} -3 & -3 & 0 \\ 0 & 0 & 0 \\ 3 & 3 & 0 \end{bmatrix}, S^y = \begin{bmatrix} 0 & 0 & 0 \\ 0 & 0 & 0 \\ 0 & 0 & 0 \end{bmatrix}, S^{xy} = \begin{bmatrix} 1 & 1 & 0 \\ 4 & 4 & 0 \\ 1 & 1 & 0 \end{bmatrix}. \tag{2.17c}$$

South: $j = 2, \ldots, N_x - 1, k = 2$ in (2.9)

$$S = \begin{bmatrix} 0 & 0 & 0 \\ 0 & 0 & 0 \\ 0 & 0 & 0 \end{bmatrix}, S^x = \begin{bmatrix} 0 & 0 & 0 \\ 0 & 0 & 0 \\ 0 & 0 & 0 \end{bmatrix}, S^y = \begin{bmatrix} 0 & 0 & 0 \\ 3 & 0 & -3 \\ 3 & 0 & -3 \end{bmatrix}, S^{xy} = \begin{bmatrix} 0 & 0 & 0 \\ 1 & 4 & 1 \\ 1 & 4 & 1 \end{bmatrix}. \tag{2.17d}$$

In summary, every interior or boundary grid point $(x_j, y_k)$ in $\Phi$ correspond to 6 difference equations with 6 unknowns $\{u_{j,k}, u^x_{j,k}, u^{xx}_{j,k}, u^y_{j,k}, u^{yy}_{j,k}, u^{xy}_{j,k}\}$; see Table 1 for details. Therefore, we can combine all these equations and form a CCD2 system. The resulting coefficient matrix is of size $(6N_xN_y)$-by-$(6N_xN_y)$ and possesses a 6-by-6 block structure with many sub-blocks being zeros and the nonzero ones being highly sparse. We remark that the block structure of this coefficient matrix is similar to (2.10) in periodic case, but each sub-block is more complex because of boundary difference equations. Therefore we have no intention of writing this matrix with some intricate notations.

A good feature of the CCD2 scheme is that all the difference equations (Table 1 minus its first row) are independent from the problem. When the subject of interest changes, we only have to alter the governing equation (2.3) and its boundary condition (2.11). Therefore about 5/6 of the resulting CCD2 coefficient matrix is fixed, owing to the fixed difference equations. This feature gives the CCD2 a huge flexibility in practical application because it requires no discretization at all.

Table 1: Corresponding difference equations for each interior and boundary grid point. In this table, 'E' stands for East , 'NE' stands for Northeast, and so on.

| Interior | Boundary | | | | | | | |
|---|---|---|---|---|---|---|---|---|
| | E | N | W | S | NE | NW | SW | SE |
| (2.3) | (2.11) | (2.11) | (2.11) | (2.11) | (2.11) | (2.11) | (2.11) | (2.11) |
| (2.4a) | (2.5a) | (2.4a) | (2.5a) | (2.4a) | (2.12a) | (2.13a) | (2.14a) | (2.12a) |
| (2.4b) | (2.5b) | (2.4b) | (2.5b) | (2.4b) | (2.12b) | (2.13b) | (2.14b) | (2.12b) |
| (2.5a) | (2.12a) | (2.13a) | (2.14a) | (2.15a) | (2.13a) | (2.14a) | (2.15a) | (2.15a) |
| (2.5b) | (2.12b) | (2.13b) | (2.14b) | (2.15b) | (2.13b) | (2.14b) | (2.15b) | (2.15b) |
| (2.8) | (2.17a) | (2.17b) | (2.17c) | (2.17d) | (2.16a) | (2.16b) | (2.16c) | (2.16d) |

**Remark 1.** *In this paper, we aim to illustrate the CCD2 scheme in a general sense, and hence the governing equation* (2.3) *is not used for boundary grid points because there is a chance that* (2.3) *disappears at the boundary. When* (2.3) *is active at the boundary, it will be a wise move to use* (2.3) *for boundary grid points and remove the complicated difference equations* (2.16) *and* (2.17) *for mixed derivative.*

**Remark 2.** *For difference equations, there are tons of finite difference equations one could use, but from our many attempts only the current group of*

*difference equations (Table 1) results in a nonsingular CCD2 system. The relation between difference equations and singularity of resulting CCD2 system still needs further investigations.*

## 3. Fourier analysis of error

Resolution characteristics is concerned with the difference between approximation and exact result. For instance, the exact values of derivatives are different from those calculated by approximations. The resolution characteristics of differential approximations is quantified by means of a Fourier analysis of the differential scheme [5, 17, 20, 28]. Through Fourier analysis, the difference is reflected by the exact wavenumbers and their approximate counterparts, which are also known as the modified wavenumbers. Similar to [5, 17, 20], we now proceed to carry out the Fourier analysis on the interior difference equations (2.4), (2.5), and (2.8). For convenience, we consider a periodic test function $u(x, y)$ over a 2D rectangular domain $[0, l_x] \times [0, l_y]$. Let $h_x$ and $h_y$ denote the mesh sizes after discretization. The dependent variable may be decomposed into Fourier series

$$u(x, y) = \sum_{p,q} \hat{u}_{p,q} e^{2\pi i p x / l_x} e^{2\pi i q y / l_y},$$

where $\hat{u}_{p,q}$ are the Fourier coefficients and $i \equiv \sqrt{-1}$. Moreover, two scaled wavenumbers are defined as

$$\mu = \frac{2\pi p h_x}{l_x} \quad \text{and} \quad \nu = \frac{2\pi q h_y}{l_y}.$$

Then $u(x, y)$ is also represented by

$$u(x, y) = \sum_{p,q} \hat{u}_{p,q} e^{i\mu x / h_x} e^{i\nu y / h_y}.$$

The Fourier coefficients of the derivatives are given exactly as

$$u^x(x, y) = \sum_{p,q} \frac{i\mu}{h_x} \hat{u}_{p,q} e^{i\mu x / h_x} e^{i\nu y / h_y},$$

$$u^y(x, y) = \sum_{p,q} \frac{i\nu}{h_y} \hat{u}_{p,q} e^{i\mu x / h_x} e^{i\nu y / h_y},$$

$$u^{xy}(x, y) = \sum_{p,q} -\frac{\mu\nu}{h_x h_y} \hat{u}_{p,q} e^{i\mu x / h_x} e^{i\nu y / h_y} \equiv \sum_{p,q} -\frac{\omega}{h_x h_y} \hat{u}_{p,q} e^{i\mu x / h_x} e^{i\nu y / h_y},$$

$$u^{xx}(x,y) = \sum_{p,q} -\left(\frac{\mu}{h_x}\right)^2 \hat{u}_{p,q} e^{i\mu x/h_x} e^{i\nu y/h_y},$$

$$u^{yy}(x,y) = \sum_{p,q} -\left(\frac{\nu}{h_y}\right)^2 \hat{u}_{p,q} e^{i\mu x/h_x} e^{i\nu y/h_y}.$$

Note that the Fourier coefficients of the approximate derivatives by the difference equations are not the same as the exact Fourier coefficients. Therefore we name these approximations as

$$\frac{i\mu'}{h_x}\hat{u}_{p,q} \approx \frac{i\mu}{h_x}\hat{u}_{p,q}, \quad \frac{i\nu'}{h_y}\hat{u}_{p,q} \approx \frac{i\nu}{h_y}\hat{u}_{p,q}, \quad -\frac{\omega'}{h_x h_y} \approx -\frac{\omega}{h_x h_y},$$

$$-\left(\frac{\mu''}{h_x}\right)^2 \hat{u}_{p,q} \approx -\left(\frac{\mu}{h_x}\right)^2 \hat{u}_{p,q}, \quad -\left(\frac{\nu''}{h_y}\right)^2 \hat{u}_{p,q} \approx -\left(\frac{\nu}{h_y}\right)^2 \hat{u}_{p,q},$$

where $\mu'$ and $\mu''$ are the modified wavenumbers for the first-order and second-order approximations in the $x$-direction respectively, and $\nu'$ and $\nu''$ are the counterparts in the $y$-direction. For the mixed derivative, the modified wavenumber is $\omega'$. Next we want to examine the difference between the exact and modified wavenumbers.

We first study the modified wavenumbers produced by the difference equations in (2.4) and (2.5). Since these equations are converted from the 1D difference equations in [5], we can find the modified wavenumbers $\mu'$, $\nu'$, $\mu''$, and $\nu''$ therein:

$$\mu' = \frac{9(4+\cos\mu)\sin\mu}{24+20\cos\mu+\cos 2\mu}, \quad \nu' = \frac{9(4+\cos\nu)\sin\nu}{24+20\cos\nu+\cos 2\nu}, \tag{3.1}$$

$$\mu'' = \sqrt{\frac{81-48\cos\mu-33\cos 2\mu}{48+40\cos\mu+2\cos 2\mu}}, \quad \text{and} \quad \nu'' = \sqrt{\frac{81-48\cos\nu-33\cos 2\nu}{48+40\cos\nu+2\cos 2\nu}}.$$

The difference between all these modified wavenumbers and the exact values are plotted in [5]. The difference equations in (2.4) and (2.5) have the closest modified wavenumbers among various high-order schemes, including the standard Padé schemes in [17]; see [5, 17] for more details.

The new member of the interior difference equations is (2.8) for mixed derivative, therefore its modified wavenumber $\omega'$ needs to be studied. Following [5], we first derive the approximate Fourier series for all the involved nodes in (2.8). Putting all these approximations into (2.8) and eliminating the common factor, we have

$$\omega' = \frac{-9\sin\mu\sin\nu + 9\nu'\sin\mu + 9\mu'\sin\nu}{8-\cos\mu\cos\nu+\cos\mu+\cos\nu},$$

where $\mu'$ and $\nu'$ given by (3.1) are functions of $\mu$ and $\nu$ respectively. Thus, the modified wavenumber $\omega'$ is also a function of $\mu$ and $\nu$. We now study the difference between the modified wavenumber $\omega'$ and the exact wavenumber $\omega = \mu\nu$. Since no other difference equation on mixed derivative is studied before, we choose to carry out the analysis on the second-order accurate (2.6) and the fourth-order accurate (2.7) for comparison. The second-order standard approximation (2.6) for the mixed derivative has a modified wavenumber

$$\omega' = \sin\mu \sin\nu,$$

while the one in the fourth-order case (2.7) is

$$\omega' = -\sin\mu \sin\nu + \nu' \sin\mu + \mu' \sin\nu.$$

Note that $\omega' = \omega'(\mu, \nu)$ is a 2D surface depending on $\mu$ and $\nu$. The goal is to observe the difference between the surfaces $\omega = \mu\nu$ and $\omega'$. The closer the modified wavenumber is, the better the spectral resolution. However, displaying a 2D figure might not be the best choice for examination. Since the two surfaces $\omega$ and $\omega'$ are symmetric about the variables $\mu$ and $\nu$, we decide to check the cross section at $\mu = \nu$. These cross sections are plotted in Figure 2. Among the three choices for approximating the mixed derivative, the sixth-order approximation (2.8) has the closest modified wavenumber.

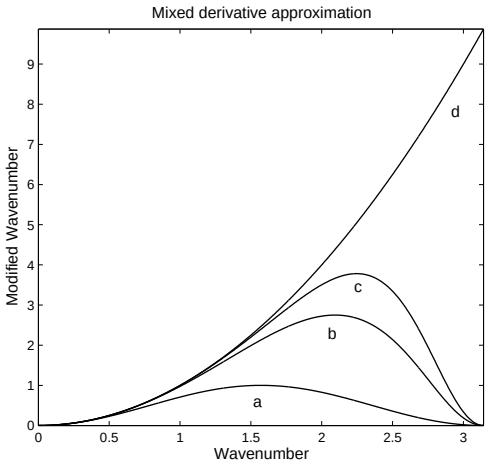


Figure 2: Fourier error analysis of difference equations for mixed derivative at $\mu = \nu$: (a) second-order difference equation (2.6); (b) fourth-order difference equation (2.7); (c) sixth-order difference equation (2.8); (d) exact wavenumber.

Other than plotting the visual difference, it is a common practice to study the resolving efficiency [17, 20], which represents the fraction of well-resolved waves within a predetermined error tolerance $\epsilon$. The resolving efficiency is then measured by $\omega_r/\pi$, such that

$$\frac{|\omega' - \omega|}{\omega} \leq \epsilon, \quad \forall \omega' \leq \omega_r.$$

The resolving efficiency in Figure 2 for $\epsilon = 0.1$, 0.01, and 0.001 is reported in Table 2. It is easy to see that the sixth-order accurate (2.8) has the largest portion of well-resolved waves in all 3 cases.

Table 2: Resolving efficiency of difference equations for mixed derivative shown in Figure 2.

| Equations | $\epsilon = 0.1$ | $\epsilon = 0.01$ | $\epsilon = 0.001$ |
|---|---|---|---|
| (2.6) | 0.24 | 0.13 | 0.07 |
| (2.7) | 0.40 | 0.27 | 0.18 |
| (2.8) | 0.52 | 0.39 | 0.29 |

## 4. Numerical experiments

In this section, we perform several numerical tests to verify the efficiency of the proposed CCD2 scheme. The universal format of (2.1) and the mixed derivative therein have frustrated many existing discretization methods. As a comparison, the standard second-order central finite difference (SOD) scheme and the FOC scheme in [15] are also employed to solve the following examples. Note that the FOC scheme is only considered in one of the examples because $\dfrac{\partial^2 u}{\partial x^2}$ and $\dfrac{\partial^2 u}{\partial y^2}$ in (2.1) are required to have identical coefficients.

For system solver, we remark that the SOD and FOC schemes are typical 2D compact schemes. There are many existing efficient solvers and we only consider the sparse direct solver for solving linear systems produced by the SOD and FOC schemes. Since the resulting system of the CCD2 scheme is highly nonsymmetric and indefinite, we solve it by the software package ILU++ [21, 22, 23], where multilevel ILU-based preconditioned BiCGStab methods are implemented.

The default configuration for the preconditioners is set to be 1, which specifies the PQ-reordering preprocessing and adopts error-based dropping

rules. We remark that this strategy may not the best for all problems. By varying the threshold parameter $\tau$ for the incomplete LU factorizations, we could better the performance of the preconditioners; see [21, 22, 23] for details. The initial guess is the zero vector and the high-precision stopping criterion is

$$\|\boldsymbol{z}_k\|_2/\|\boldsymbol{z}_0\|_2 \leq 10^{-10} \quad \text{and} \quad \|\boldsymbol{z}_k\|_2 \leq 10^{-10},$$

where $\boldsymbol{z}_k$ is the residual vector at the $k$th iteration. Since choosing the optimal $\tau$ is very problem-dependent, our given selections are based on experimental observations and not discreetly optimized.

To demonstrate the edge of the CCD2 scheme in handling (2.1), we report the orders of accuracy in approximate solutions as well as their partial derivatives. A square domain is considered in the following experiments, therefore we let $N = N_x = N_y$ be the number of grid points in both directions and $h = \frac{1}{N-1} = h_x = h_y$ be the mesh size. We symbolize the approximate solution with mesh size $h$ by $u_h$. The error of the approximate solution is measured under the infinity norm

$$e_h \equiv \|u - u_h\|_\infty = \max_{1\leq j,k\leq N} |u(x_j, y_k) - u_h(x_j, y_k)|$$

and the corresponding order of accuracy is calculated as

$$\text{Rate} = \log_2\left(\frac{e_{2h}}{e_h}\right).$$

Analogously, the notations $e_h^x$, $e_h^y$, $e_h^{xx}$, $e_h^{yy}$, and $e_h^{xy}$ are the approximate errors of $u_h^x$, $u_h^y$, $u_h^{xx}$, $u_h^{yy}$, and $u_h^{xy}$, respectively.

*4.1. Example 1 with variable coefficients* [3]

The first model problem is defined on the unit square $\Omega = [0, 1]^2$ with $\mathsf{D} = [x + 2, -y]$, $\alpha = 0$, and full tensor coefficient

$$\mathsf{K} = \begin{bmatrix} (x+1)^2 + y^2 & -xy \\ -xy & (x+1)^2 \end{bmatrix}$$

in (1.1). The corresponding elliptic equation reads

$$\left[(x+1)^2 + y^2\right] \frac{\partial^2 u}{\partial x^2} - 2xy\frac{\partial^2 u}{\partial x \partial y} + (x+1)^2\frac{\partial^2 u}{\partial y^2} + (x+2)\frac{\partial u}{\partial x} - y\frac{\partial u}{\partial y} = g(x, y), \tag{4.1}$$

where $g(x, y)$ is chosen accordingly such that the true solution is

$$u = x^3y^2 + x\sin(x)\cos(xy). \tag{4.2}$$

We consider solving (4.1) with Dirichlet and Robin boundary conditions. The Dirichlet boundary condition is taken from the exact solution (4.2), while the Robin boundary condition is given by

$$\begin{cases} \dfrac{\partial u}{\partial x} = \hat{u}, & (x,y) \in \Psi \equiv 0 \times [0,1], \\ u = x^3y^2 + x\sin(x)\cos(xy), & (x,y) \in \partial\Omega \backslash \Psi, \end{cases}$$

where

$$\begin{aligned} \hat{u} &= \frac{\partial}{\partial x}\left[x^3y^2 + x\sin(x)\cos(xy)\right] \\ &= 3x^2y^2 + \sin(x)\cos(xy) + x\cos(x)\cos(xy) - xy\sin(x)\sin(xy). \end{aligned}$$

The numerical results for both boundary conditions are given in Table 3, in which the SOD scheme is also used. These results show that the CCD2 scheme is sixth-order accurate with Dirichlet boundary condition, and the SOD scheme is acting normal with its second-order accuracy. Note that the resulting coefficient matrix of the CCD2 scheme is approximately 6 times as large as the one produced by the SOD scheme. However, we clearly see from numerical results that the high-order accurate CCD2 scheme achieves a similar accuracy level with a much coarser grid than the SOD scheme.

On the other hand, without any additional treatment for the boundary difference equations, we observe from Table 3 that the CCD2 scheme is only fifth-order accurate for approximating the true solution with the presence of Robin boundary condition. We remark that the fifth-order accuracy of approximate solution is relatively competent, and the recovery of sixth-order accuracy is not the focus of this paper.

Since the approximate partial derivatives are the byproducts of the CCD2 scheme, we also report in Table 4 their errors when solving (4.1) with Dirichlet boundary condition. We observe that the approximate partial derivatives are at least fourth-order accurate.

*4.2. Example 2 with high anisotropy ratio* [6]

The second model problem is also defined on the unit square $\Omega = [0,1]^2$ with $\mathsf{D} = [(3\varepsilon - 1)x, (3\varepsilon - 1)y]$, $\alpha = 0$, and full tensor coefficient

$$\mathsf{K} = \begin{bmatrix} \varepsilon x^2 + y^2 & -(1-\varepsilon)xy \\ -(1-\varepsilon)xy & x^2 + \varepsilon y^2 \end{bmatrix}$$

in (1.1), where $0 < \varepsilon \leq 1$ is an anisotropy parameter. Note that $\varepsilon = 1$ gives an isotropic equation, and the degree of anisotropy increases when $\varepsilon$

Table 3: Errors and orders of accuracy in Example 1: Dirichlet and Robin boundary conditions.

| | Dirichlet | | | | Robin | | | |
|---|---|---|---|---|---|---|---|---|
| | SOD | | CCD2 | | SOD | | CCD2 | |
| $1/h$ | $e_h$ | Rate | $e_h$ | Rate | $e_h$ | Rate | $e_h$ | Rate |
| 8 | 7.46e-04 | | 5.97e-06 | | 4.24e-03 | | 7.52e-05 | |
| 16 | 1.91e-04 | 1.96 | 1.56e-07 | 5.26 | 1.20e-03 | 1.83 | 2.74e-06 | 4.78 |
| 32 | 4.80e-05 | 2.00 | 3.14e-09 | 5.63 | 3.18e-04 | 1.91 | 9.12e-08 | 4.91 |
| 64 | 1.20e-05 | 2.00 | 5.75e-11 | 5.77 | 8.21e-05 | 1.95 | 2.92e-09 | 4.96 |
| 128 | 3.00e-06 | 2.00 | | | 2.08e-05 | 1.98 | | |
| 256 | 7.50e-07 | 2.00 | | | 5.25e-06 | 1.99 | | |
| 512 | 1.88e-07 | 2.00 | | | 1.32e-06 | 1.99 | | |

Table 4: Errors of approximate partial derivatives in Example 1: Dirichlet boundary condition.

| $1/h$ | $e_h^x$ | Rate | $e_h^y$ | Rate | $e_h^{xx}$ | Rate | $e_h^{yy}$ | Rate | $e_h^{xy}$ | Rate |
|---|---|---|---|---|---|---|---|---|---|---|
| 8 | 3.7e-04 | | 9.3e-05 | | 1.1e-02 | | 1.0e-03 | | 2.0e-03 | |
| 16 | 1.5e-05 | 4.6 | 4.0e-06 | 4.5 | 8.7e-04 | 3.6 | 7.9e-05 | 3.7 | 2.1e-04 | 3.3 |
| 32 | 5.5e-07 | 4.8 | 1.4e-07 | 4.8 | 6.1e-05 | 3.8 | 5.4e-06 | 3.9 | 1.6e-05 | 3.7 |
| 64 | 1.9e-08 | 4.9 | 4.8e-09 | 4.9 | 4.0e-06 | 3.9 | 3.5e-07 | 3.9 | 1.1e-06 | 3.9 |

becomes smaller. The corresponding explicit equation reads

$$\begin{aligned}(\varepsilon x^2+y^2)\frac{\partial^2 u}{\partial x^2}+2(\varepsilon-1)xy\frac{\partial^2 u}{\partial x\partial y}+(x^2+\varepsilon y^2)\frac{\partial^2 u}{\partial y^2}&\\ +(3\varepsilon-1)x\frac{\partial u}{\partial x}+(3\varepsilon-1)y\frac{\partial u}{\partial y} &= g(x,y),\quad (4.3)\end{aligned}$$

where $g(x,y)$ is chosen according to the true solution

$$u=\sin(\pi x)\sin(\pi y).$$

The Dirichlet boundary condition is set by restricting the true solution on $\partial\Omega$. The approximate errors of applying the CCD2 scheme to (4.3) are presented in Table 5 with different sizes of anisotropy ratio $\varepsilon$. Numerical results show that our proposed CCD2 scheme is seventh-order accurate and its excellent performance is obviously independent of the anisotropy ratio $\varepsilon=10^{-1}$ and $10^{-3}$, which is a rare phenomenon for high-order schemes and thus very attractive in real-life applications.

Table 5: Errors and orders of accuracy in Example 2: $\varepsilon = 10^{-1}$ and $\varepsilon = 10^{-3}$.

| | $\varepsilon = 10^{-1}$ | | | | $\varepsilon = 10^{-3}$ | | | |
|---|---|---|---|---|---|---|---|---|
| | SOD | | CCD2 | | SOD | | CCD2 | |
| $1/h$ | $e_h$ | Rate | $e_h$ | Rate | $e_h$ | Rate | $e_h$ | Rate |
| 8 | 1.31e-02 | | 1.27e-04 | | 1.54e-02 | | 1.67e-04 | |
| 16 | 3.42e-03 | 1.94 | 1.09e-06 | 6.87 | 4.23e-03 | 1.86 | 1.12e-06 | 7.21 |
| 32 | 8.52e-04 | 2.00 | 8.71e-09 | 6.96 | 1.06e-03 | 2.00 | 8.80e-09 | 6.99 |
| 64 | 2.13e-04 | 2.00 | 6.87e-11 | 6.99 | 2.66e-04 | 1.99 | 6.90e-11 | 7.00 |
| 128 | 5.32e-05 | 2.00 | | | 6.64e-05 | 2.00 | | |
| 256 | 1.33e-05 | 2.00 | | | 1.66e-05 | 2.00 | | |
| 512 | 3.33e-06 | 2.00 | | | 4.15e-06 | 2.00 | | |

*4.3. Example 3 with large Reynolds number* [15]

The third model problem is also defined on the unit square $\Omega = [0,1]^2$, and the governing equation is

$$\begin{aligned} &\frac{\partial^2 u}{\partial x^2} + \cos(\pi x)\sin(\pi y)\frac{\partial^2 u}{\partial x \partial y} + \frac{\partial^2 u}{\partial y^2} \\ -\mathrm{Re}(1-x)(1-2y)\frac{\partial u}{\partial x} + 4\mathrm{Re}\cdot xy(1-y)\frac{\partial u}{\partial y} &= g(x,y) \end{aligned}$$

with the forcing term $g(x,y)$ being chosen such that the true solution is

$$u = \sin(\pi x) + \sin(\pi y) + \sin(\pi x)\sin(\pi y),$$

which does not depend on the so-called Reynolds number Re. The Dirichlet boundary condition is set by restricting the true solution on $\partial\Omega$. In this example, we also consider the fourth-order accurate FOC scheme developed in [15] besides the SOD scheme.

The approximate errors for the case $\mathrm{Re} = 10^2, 10^4$, and $10^6$ are given in Table 6, 7, and 8, respectively. Here we observe that the SOD and CCD2 schemes are almost not influenced by the increase of Reynolds number, while the FOC scheme gradually loses its fourth-order accuracy. This numerical phenomenon was also noted in [30] when the original CCD scheme [5] was applied to a 1D convection diffusion equation. However, the emphasis is more about the oscillation property of the CCD scheme when treating boundary layers in [30]. In contrast, we straighten out that the CCD\CCD2's insensitiveness to Reynolds number puts it in a better position over other HOC schemes, including the FOC scheme in [15], which fails to keep its

fourth-order accuracy when the Reynolds number approaches $10^4$. We remark that nonuniform grids [12] or local mesh refinement strategy could be employed to alleviate the numerical oscillations of the CCD2 scheme when facing boundary layer problems, but it is beyond the scope of the current work.

Table 6: Errors and orders of accuracy in Example 3 with $\mathrm{Re} = 10^2$.

| | SOD | | FOC | | CCD2 | |
|---|---|---|---|---|---|---|
| $1/h$ | $e_h$ | Rate | $e_h$ | Rate | $e_h$ | Rate |
| 8 | 5.49e-02 | | 8.56e-03 | | 3.93e-04 | |
| 16 | 1.41e-02 | 1.97 | 6.49e-04 | 3.72 | 3.08e-06 | 6.99 |
| 32 | 3.53e-03 | 1.99 | 4.09e-05 | 3.99 | 2.11e-08 | 7.19 |
| 64 | 8.86e-04 | 2.00 | 2.56e-06 | 4.00 | 1.48e-10 | 7.16 |
| 128 | 2.22e-04 | 2.00 | 1.60e-07 | 4.00 | | |
| 256 | 5.54e-05 | 2.00 | 1.00e-08 | 4.00 | | |
| 512 | 1.39e-05 | 2.00 | 6.26e-10 | 4.00 | | |

Table 7: Errors and orders of accuracy in Example 3 with $\mathrm{Re} = 10^4$.

| | SOD | | FOC | | CCD2 | |
|---|---|---|---|---|---|---|
| $1/h$ | $e_h$ | Rate | $e_h$ | Rate | $e_h$ | Rate |
| 8 | 6.48e-02 | | 1.50e-02 | | 4.17e-04 | |
| 16 | 1.72e-02 | 1.92 | 4.89e-03 | 1.62 | 4.38e-06 | 6.57 |
| 32 | 4.36e-03 | 1.98 | 1.74e-03 | 1.49 | 3.84e-08 | 6.84 |
| 64 | 1.05e-03 | 2.05 | 2.81e-04 | 2.63 | 3.28e-10 | 6.87 |
| 128 | 2.63e-04 | 2.00 | 1.96e-05 | 3.84 | | |
| 256 | 6.63e-05 | 1.99 | 1.21e-06 | 4.01 | | |
| 512 | 1.66e-05 | 2.00 | 7.57e-08 | 4.00 | | |

Previously we have only put our attention to the convergence rate of the CCD2 scheme. Now we proceed to examine the performance of the ILU preconditioned BiCGStab solver [21, 22, 23]. The iteration numbers and computation time (in seconds) of the ILU preconditioned BiCGStab solver for all examples are shown in Table 9 and 10, respectively. In the ILU preconditioned BiCGStab algorithm, the threshold $\tau$ is utilized to preserve sparsity by dropping those smaller nonzero elements during the incomplete LU factorizations; see [23]. In our numerical experiments, smaller $\tau$'s are used for larger Reynolds numbers in order to achieve the expected high-order accuracy. We point out that the computation time is determined by

Table 8: Errors and orders of accuracy in Example 3 with $\mathrm{Re} = 10^6$.

| | SOD | | FOC | | CCD2 | |
|---|---|---|---|---|---|---|
| $1/h$ | $e_h$ | Rate | $e_h$ | Rate | $e_h$ | Rate |
| 8 | 6.48e-02 | | 1.50e-02 | | 4.16e-04 | |
| 16 | 1.72e-02 | 1.91 | 4.82e-03 | 1.63 | 4.29e-06 | 6.60 |
| 32 | 4.43e-03 | 1.96 | 1.84e-03 | 1.39 | 3.55e-08 | 6.92 |
| 64 | 1.13e-03 | 1.97 | 6.21e-04 | 1.56 | 2.87e-10 | 6.95 |
| 128 | 2.82e-04 | 2.00 | 1.98e-04 | 1.65 | | |
| 256 | 7.05e-05 | 2.00 | 5.63e-05 | 1.81 | | |
| 512 | 1.75e-05 | 2.01 | 7.82e-06 | 2.85 | | |

the iteration number as well as the setup of preconditioner.

Table 9: Number of ILU preconditioned BiCGStab iterations for all examples.

| | Example 1 | | Example 2 | | Example 3 | | |
|---|---|---|---|---|---|---|---|
| | Dirichlet | Robin | $\varepsilon = 10^{-1}$ | $\varepsilon = 10^{-3}$ | $\mathrm{Re} = 10^2$ | $\mathrm{Re} = 10^4$ | $\mathrm{Re} = 10^6$ |
| $1/h$ | $\tau = 10^{-2}$ | $\tau = 10^{-3}$ | $\tau = 10^{-3}$ | $\tau = 10^{-3}$ | $\tau = 10^{-3}$ | $\tau = 10^{-4}$ | $\tau = 10^{-6}$ |
| 8 | 29 | 9 | 13 | 15 | 15 | 26 | 41 |
| 16 | 33 | 12 | 17 | 26 | 14 | 30 | 58 |
| 32 | 37 | 15 | 23 | 31 | 14 | 15 | 30 |
| 64 | 53 | 39 | 22 | 45 | 17 | 13 | 13 |

Table 10: Computation time of ILU preconditioned BiCGStab solvers for all examples.

| | Example 1 | | Example 2 | | Example 3 | | |
|---|---|---|---|---|---|---|---|
| | Dirichlet | Robin | $\varepsilon = 10^{-1}$ | $\varepsilon = 10^{-3}$ | $\mathrm{Re} = 10^2$ | $\mathrm{Re} = 10^4$ | $\mathrm{Re} = 10^6$ |
| $1/h$ | $\tau = 10^{-2}$ | $\tau = 10^{-3}$ | $\tau = 10^{-3}$ | $\tau = 10^{-3}$ | $\tau = 10^{-3}$ | $\tau = 10^{-4}$ | $\tau = 10^{-6}$ |
| 8 | 0.02 | 0.02 | 0.05 | 0.05 | 0.04 | 0.03 | 0.04 |
| 16 | 0.11 | 0.31 | 0.45 | 0.42 | 0.33 | 0.25 | 0.28 |
| 32 | 0.61 | 1.27 | 1.80 | 1.84 | 2.08 | 1.34 | 1.76 |
| 64 | 3.32 | 8.52 | 8.07 | 9.46 | 11.93 | 14.16 | 13.27 |

## 5. Concluding remarks

In this work we have set up an implementation framework of the CCD2 scheme (2D CCD scheme), with the existence of mixed derivative term. Numerical results exhibit the remarkable performance of the CCD2 scheme, which obtains high-order accurate solutions as well as derivatives, and is relatively competent with high Reynolds numbers.

There are certain issues up ahead. Boundary layer problems are challenging for designing high-order schemes and require certain local mesh refinement strategy, which is highly adaptive to the 9-point CCD2 scheme. Furthermore, 2D parabolic equations with a mixed derivative term will also be considered. The temporal integration needs as much attention in order to achieve high-order accuracy in both space and time.

Some might argue that implicit HOC schemes like the CCD and CCD2 schemes require additional computational costs since they include the derivatives as unknowns while these derivatives are not wanted. We remark that the implicit treatment is the means to high-order accuracy, and the numerical results show that the CCD2 scheme achieves high-order accurate approximations with an extremely coarse grid. On the other hand, there are certain applications which require the computations of derivatives. For instance, Navier-Stokes equations require both derivatives of most variables [20]. Also in computational finance, the option pricing problem in the stochastic volatility with correlated and contemporaneous jumps in return and variance (SVCJ) model [9] is formulated as a 2D partial integro-differential equation (PIDE) with a mixed derivative. Apart from solving this PIDE efficiently, all the derivatives which are known as the Greeks, have their own financial meanings and require accurate computations. These kinds of applications will be on top of our to-do list.

# Appendices

### Appendix A. Derivation of (2.6), (2.7), and (2.8)

We first show how to obtain the difference equations (2.6), (2.7), and (2.8) for the mixed derivative. Define the following notation

$$u^{(m,n)} \equiv \frac{\partial^{m+n} u}{\partial x^m \partial y^n}.$$

For simplicity, we assume $\{u^x, u^{xx}, u^y, u^{yy}, u^{xy}\}$ follow the above notation, for instance, $u^{(1,1)}$ represents $u^{xy}$. All the other notations are consistent

with the paper. From the 2D Taylor expansion, it is easy to see that

$$\begin{aligned} u_{j,k}^{(1,1)} &= \frac{1}{4h_xh_y}(u_{j+1,k+1}+u_{j-1,k-1}-u_{j-1,k+1}-u_{j+1,k-1}) - \frac{h_x^2}{6}u_{j,k}^{(3,1)} \\ &\quad -\frac{h_y^2}{6}u_{j,k}^{(1,3)} - \frac{h_x^4}{120}u_{j,k}^{(5,1)} - \frac{h_x^2h_y^2}{36}u_{j,k}^{(3,3)} - \frac{h_y^4}{120}u_{j,k}^{(1,5)} + \mathcal{O}(h_x^6+h_y^6), \end{aligned} \tag{A.1}$$

which is the standard approximation (2.6) for mixed derivative if the high-order terms are ignored. A technical maneuver enables us to eliminate the terms $u_{j,k}^{(5,1)}$ and $u_{j,k}^{(1,5)}$ first. From 1D viewpoint, we have the following Taylor expansion in the $x$-direction:

$$u_{j,k}^{(1,0)} = \frac{1}{2h_x}(u_{j+1,k}-u_{j-1,k}) - \frac{h_x^2}{6}u_{j,k}^{(3,0)} - \frac{h_x^4}{120}u_{j,k}^{(5,0)} + \mathcal{O}(h_x^6).$$

We replace $u_{j,k}$ by $u_{j,k}^{(0,1)}$ to derive

$$\frac{h_x^2}{6}u_{j,k}^{(3,1)} = \frac{1}{2h_x}\left(u_{j+1,k}^{(0,1)}-u_{j-1,k}^{(0,1)}\right) - u_{j,k}^{(1,1)} - \frac{h_x^4}{120}u_{j,k}^{(5,1)} + \mathcal{O}(h_x^6). \tag{A.2}$$

Similarly we have the following equation in another direction

$$\frac{h_y^2}{6}u_{j,k}^{(1,3)} = \frac{1}{2h_y}\left(u_{j,k+1}^{(1,0)}-u_{j,k-1}^{(1,0)}\right) - u_{j,k}^{(1,1)} - \frac{h_y^4}{120}u_{j,k}^{(1,5)} + \mathcal{O}(h_y^6). \tag{A.3}$$

Putting the sixth-order accurate (A.2) and (A.3) into (A.1), we observe that the terms $u_{j,k}^{(5,1)}$ and $u_{j,k}^{(1,5)}$ disappear. If we just stop here, then the fourth-order accurate (2.7) is derived. To obtain the sixth-order accurate (2.8), we have to take care of the term $u_{j,k}^{(3,3)}$.

Note that there exists the following well-known approximation to $u_{j,k}^{(2,2)}$:

$$\begin{aligned} u_{j,k}^{(2,2)} &= \frac{1}{h_x^2h_y^2}(-2u_{j+1,k}-2u_{j,k+1}-2u_{j-1,k}-2u_{j,k-1} \\ &\quad +u_{j+1,k+1}+u_{j-1,k+1}+u_{j-1,k-1}+u_{j+1,k-1}+4u_{j,k}) + \mathcal{O}(h_x^2+h_y^2). \end{aligned}$$

We then replace $u_{j,k}$ by $u_{j,k}^{(1,1)}$ to get

$$\begin{aligned} u_{j,k}^{(3,3)} &= \frac{1}{h_x^2h_y^2}\Big(-2u_{j+1,k}^{(1,1)}-2u_{j,k+1}^{(1,1)}-2u_{j-1,k}^{(1,1)}-2u_{j,k-1}^{(1,1)} \\ &\quad +u_{j+1,k+1}^{(1,1)}+u_{j-1,k+1}^{(1,1)}+u_{j-1,k-1}^{(1,1)}+u_{j+1,k-1}^{(1,1)}+4u_{j,k}^{(1,1)}\Big) \\ &\quad +\mathcal{O}(h_x^2+h_y^2). \end{aligned} \tag{A.4}$$

Putting (A.2), (A.3), and (A.4) into (A.1), we ultimately obtain the sixth-order accurate difference equation (2.8).

## Appendix B. Truncation errors of difference equations

Here we display the truncation errors in various difference equations used in this paper. Note that the difference equations (2.4) and (2.5) exist in the previous literature [5] and their truncation errors can be found therein.

Table B.11: Truncation errors in various difference equations.

| | Equations | Truncation errors |
|---|---|---|
| Interior | (2.6) | $\frac{1}{6}\left\|u^{(3,1)}\right\| h_x^2 + \frac{1}{6}\left\|u^{(1,3)}\right\| h_y^2$ |
| | (2.7) | $\frac{1}{36}\left\|u^{(3,3)}\right\| h_x^2 h_y^2$ |
| | (2.8) | $\frac{1}{960}\left\|u^{(5,3)}\right\| h_x^4 h_y^2 + \frac{1}{960}\left\|u^{(3,5)}\right\| h_x^2 h_y^4$ |
| Boundary | (2.12a), (2.14a) | $\frac{1}{90}\left\|u^{(6,0)}\right\| h_x^4$ |
| | (2.12b), (2.14b) | $\frac{1}{20}\left\|u^{(6,0)}\right\| h_x^4$ |
| | (2.13a), (2.15a) | $\frac{1}{90}\left\|u^{(0,6)}\right\| h_y^4$ |
| | (2.13b), (2.15b) | $\frac{1}{20}\left\|u^{(0,6)}\right\| h_y^4$ |
| | (2.16) | $\frac{1}{36}\left\|u^{(3,3)}\right\| h_x^2 h_y^2$ |
| | (2.17a), (2.17c) | $\frac{1}{15}\left\|u^{(1,5)}\right\| h_y^4$ |
| | (2.17b), (2.17d) | $\frac{1}{15}\left\|u^{(5,1)}\right\| h_x^4$ |

## References


[1] J. Adams, P. Smolarkiewicz, Modified multigrid for 3D elliptic equations with cross-derivatives, Appl. Math. Comput. 121 (2001) 301–312.

[2] T. Arbogast, M. Wheeler, I. Yotov, Mixed finite elements for elliptic problems with tensor coefficients as cell-centered finite differences, SIAM J. Numer. Anal. 34 (1997) 828–852.

[3] M. Berndt, K. Lipnikov, M. Shashkov, M. Wheeler, I. Yotov, Superconvergence of the velocity in mimetic finite difference methods on quadrilaterals, SIAM J. Numer. Anal. 43 (2005) 1728–1749.

[4] R. Chan, X. Jin, An Introduction to Iterative Toeplitz Solvers, SIAM, Philadelphia, PA, 2007.

[5] P. Chu, C. Fan, A three-point combined compact difference scheme, J. Comput. Phys. 140 (1998) 370–399.

[6] P. Crumpton, G. Shaw, A. Ware, Discretisation and multigrid solution of elliptic equations with mixed derivative terms and strongly discontinuous coefficients, J. Comput. Phys. 116 (1995) 343–358.

[7] T. Dohnal, Perfectly matched layers for coupled nonlinear Schrödinger equations with mixed derivatives, J. Comput. Phys. 228 (2009) 8752–8765.

[8] R. Dunne, E. O'Riordan, G. Shishkin, Fitted mesh numerical methods for singularly perturbed elliptic problems with mixed derivatives, IMA J. Numer. Anal. 29 (2009) 712–730.

[9] L. Feng, V. Linetsky, Pricing options in jump-diffusion models: An extrapolation approach, Oper. Res. 56 (2008) 304–325.

[10] M. Fournié, S. Karaa, Iterative methods and high-order difference schemes for 2D elliptic problems with mixed derivative, J. Appl. Math. Comput. 22 (2006) 349–363.

[11] H. Friis, M. Edwards, J. Mykkeltveit, Symmetric positive definite flux-continuous full-tensor finite-volume schemes on unstructured cell-centered triangular grids, SIAM J. Sci. Comput. 31 (2008) 1192–1220.

[12] L. Ge, J. Zhang, High accuracy iterative solution of convection diffusion equation with boundary layers on nonuniform grids, J. Comput. Phys. 171 (2001) 560–578.

[13] G. Golub, C. Van Loan, Matrix Computations, Johns Hopkins University Press, Baltimore, MD, 1996.

[14] C. Grossmann, H.-G. Roos, M. Stynes, Numerical Treatment of Partial Differential Equations, Springer, 2007.

[15] S. Karaa, High-order difference schemes for 2D elliptic and parabolic problems with mixed derivatives, Numer. Methods Partial Differential Equations 23 (2007) 366–378.

[16] S. Karaa, M. Othman, Two-level compact implicit schemes for three-dimensional parabolic problems, Comput. Math. Appl. 58 (2009) 257–263.

[17] S. Lele, Compact finite difference schemes with spectral-like resolution, J. Comput. Phys. 103 (1992) 16–42.

[18] R. LeVeque, Finite Difference Methods for Ordinary and Partial Differential Equations, SIAM, Philadelphia, PA, 2007.

[19] R. Lynch, J. Rice, High accuracy finite difference approximation to solutions of elliptic partial differential equations, Proc. Nat. Acad. Sci. U.S.A. 75 (1978) 2541–2544.

[20] K. Mahesh, A family of high order finite difference schemes with good spectral resolution, J. Comput. Phys. 145 (1998) 332–358.

[21] J. Mayer, ILU++. `http://iamlasun8.mathematik.uni-karlsruhe.de/~ae04/iluplusplus.html`.

[22] J. Mayer, Symmetric permutations for i-matrices to delay and avoid small pivots during factorization, SIAM J. Sci. Comput. 30 (2008) 982–996.

[23] J. Mayer, A numerical evaluation of preprocessing and ilu-type preconditioners for the solution of unsymmetric sparse linear systems using iterative methods, ACM Trans. Math. Softw. 36 (2009), 1–26.

[24] D. Peaceman, Fundamentals of Numerical Reservoir Simulation, Elsevier Science Inc., New York, NY, USA, 1991.

[25] G. Pitts, C. Ribbens, Hodiex: A sixth order accurate method for solving elliptical PDEs, tech. report, Blacksburg, VA, USA, 1993.

[26] T. Sengupta, V. Lakshmanan, V. Vijay, A new combined stable and dispersion relation preserving compact scheme for non-periodic problems, J. Comput. Phys. 228 (2009) 3048–3071.

[27] T. Sengupta, V. Vijay, S. Bhaumik, Further improvement and analysis of ccd scheme: Dissipation discretization and de-aliasing properties, J. Comput. Phys. 228 (2009) 6150–6168.

[28] R. Vichnevetsky, J. Bowles, Fourier Analysis of Numerical Approximations of Hyperbolic Equations, SIAM, Philadelphia, PA, 1982.

[29] T. Yamamoto, Toward the sinc-Galerkin method for the Poisson problem in one type of curvilinear coordinate domain, Electron. Trans. Numer. Anal. 23 (2006) 63–75.

[30] J. Zhang, J. Zhao, Truncation error and oscillation property of the combined compact difference scheme, Appl. Math. Comput. 161 (2005) 241–251.